THE JOURNAL OF BIOLOGICAL CHEMISTRY VOL. 286, NO. 26, pp. 23266–23279, July 1, 2011

LFR1 Ferric Iron Reductase of *Leishmania amazonensis* Is Essential for the Generation of Infective Parasite Forms*[S]

Received for publication, February 10, 2011, and in revised form, April 22, 2011 Published, JBC Papers in Press, May 10, 2011, DOI 10.1074/jbc.M111.229674

Andrew R. Flannery[‡], Chau Huynh[‡], Bidyottam Mittra[‡], Renato A. Mortara[§], and Norma W. Andrews[‡1]

From the [‡]Department of Cell Biology and Molecular Genetics, University of Maryland, College Park, Maryland 20742-5815 and the [§]Department of Microbiology, Immunology, and Parasitology, Universidade Federal de São Paulo, 04023-062 São Paulo, Brazil

The protozoan parasite *Leishmania* is the causative agent of serious human infections worldwide. The parasites alternate between insect and vertebrate hosts and cause disease by invading macrophages, where they replicate. Parasites lacking the ferrous iron transporter LIT1 cannot grow intracellularly, indicating that a plasma membrane-associated mechanism for iron uptake is essential for the establishment of infections. Here, we identify and functionally characterize a second member of the *Leishmania* iron acquisition pathway, the ferric iron reductase LFR1. The *LFR1* gene is up-regulated under iron deprivation and accounts for all the detectable ferric reductase activity exposed on the surface of *Leishmania amazonensis*. *LFR1* null mutants grow normally as promastigote insect stages but are defective in differentiation into the vertebrate infective forms, metacyclic promastigotes and amastigotes. *LFR1* overexpression partially restores the abnormal morphology of infective stages but markedly reduces parasite viability, precluding its ability to rescue *LFR1* null replication in macrophages. However, *LFR1* overexpression is not toxic for amastigotes lacking the ferrous iron transporter LIT1 and rescues their growth defect. In addition, the intracellular growth of both *LFR1* and *LIT1* null parasites is rescued in macrophages loaded with exogenous iron. This indicates that the Fe^{3+} reductase LFR1 functions upstream of LIT1 and suggests that *LFR1* overexpression results in excessive Fe^{2+} production, which impairs parasite viability after intracellular transport by LIT1.

Human infections with the protozoan parasite *Leishmania* spp. represent a serious public health problem. Depending on the parasite species, the clinical symptoms can range from self-healing cutaneous lesions to severe visceralizing disease, which is fatal if left untreated. Control of disease transmission is very challenging, because the parasite is transmitted by several sand fly species, which are present throughout the world in both rural and urban environments (1). No vaccines are currently available, and there is a strong need for less toxic drugs for the treatment of human and animal infections. The identification of essential parasite nutrient uptake pathways is therefore of paramount importance for the development of novel therapeutic strategies. Iron is one of the four most abundant elements in the Earth's crust, but its uptake is a challenging problem for living cells (2). Iron is an essential co-factor for many enzymatic activities, and therefore it must be transported from the extracellular environment into the cytosol. However, the ferrous iron (Fe^{2+}) that is soluble at neutral pH cannot be allowed to accumulate, because it generates highly toxic radicals in the presence of oxygen (3). For this reason, in aerobic environments iron is found mostly in the poorly soluble oxidized ferric form (Fe^{3+}) and stored as a complex with iron-binding proteins such as transferrin, lactoferrin, or ferritin. Prior to transport across membranes, Fe^{3+} must be converted to Fe^{2+} by a ferric iron reductase (4, 5).

Until recently, very little was known about the mechanism by which *Leishmania* deals with the problem of iron acquisition. An important advance was the identification and characterization of LIT1, a *Leishmania amazonensis* plasma membrane Fe^{2+} transporter. LIT1 is expressed by amastigotes replicating within the low iron environment of macrophage phagolysosomes and is required for parasite replication and lesion formation *in vivo* (6–8). The process by which *Leishmania* gains access to Fe^{2+}, the LIT1 substrate, was suggested by an earlier study that detected NADPH-dependent reductase activity in *Leishmania chagasi* (9). In this work, we identify *LFR1*, a *Leishmania* gene that encodes a membrane protein with ferric reductase activity that acts in concert with the ferrous iron transporter LIT1. The ferric reductase activity of LFR1 can be detected on the cell surface of several *Leishmania* species and is required for the differentiation of *L. amazonensis* into forms capable of initiating infections in the mammalian host.

EXPERIMENTAL PROCEDURES

Parasites—L. amazonensis (IFLA/BR/67/PH8), *Leishmania major* (clone VI, MHOM/IL/80/Friedlin), *Leishmania infantum* (Spain isolate), *L. chagasi* (Brazil isolate), and *Leishmania donovani* (India isolate, MHOM/IN/83/mongi-142) were provided by D. L. Sacks (Laboratory of Parasitic Diseases, NIAID, National Institutes of Health). *L. amazonensis* Δ*lit1* was previously described (7). Promastigotes were maintained *in vitro* at 26 °C in promastigote media as follows: M199 (Invitrogen), 40 mM HEPES, pH 7.4, 20% heat-inactivated FBS, 5% penicillin/streptomycin, 0.1% hemin (from a 25 mg/ml stock in 50% triethanolamine), 10 mM adenine, and 5 mM L-glutamine. To generate *L. amazonensis* axenic amastigotes, log phase promastigotes were inoculated at 1×10^6 parasites/ml into amastigote

* This work was supported, in whole or in part, by National Institutes of Health Grant R01 AI067979 (to N. W. A.).

[S] The on-line version of this article (available at http://www.jbc.org) contains supplemental Figs. 1–3 and Table 1.

The nucleotide sequence(s) reported in this paper has been submitted to the GenBank™/EBI Data Bank with accession number(s) JF830585.

[1] To whom correspondence should be addressed: Dept. of Cell Biology and Molecular Genetics, 2134 Bioscience Research Bldg., University of Maryland, College Park, MD 20742-5815. Tel.: 301-405-9601; Fax: 301-314-1248; E-mail: andrewsn@umd.edu.

media (M199, 40 mM sodium succinate, pH 4.5, 20% heat-inactivated FBS, 5% penicillin/streptomycin, 0.1% hemin, 10 mM adenine, 5 mM L-glutamine, 0.25% glucose, and 0.5% trypticase) and incubated at 32 °C. *L. amazonensis* metacyclic forms were purified from 7-day-old promastigote stationary phase cultures using the 3A.1 mAb, which specifically agglutinates *L. amazonensis* procyclic promastigotes but not the metacyclic forms (10, 11). Parasites were washed twice with PBS, resuspended at 1.0×10^8 parasites/ml in 1.0 ml of PBS containing a 1:30 dilution of 3A.1 culture supernatant for 30 min, and centrifuged at $250 \times g$ for 5 min. Nonagglutinated parasites in the supernatant were washed twice and counted.

Identification and Cloning of LFR1 in L. amazonensis—Protein BLAST homology searches of the *L. major* data base were used to identify LmjF30.1610, which shared 36% identity and 45% similarity to the *Arabidopsis thaliana* ferric reduction oxidase 1, *FRO1.* Primers AFPNA10 and AFPNA11 (supplemental Table S1) were designed based on the LmjF30.1610 DNA sequence to amplify the predicted open reading frame (ORF) of the putative ferric reductase gene from genomic DNA of *L. amazonensis*. Genomic DNA was isolated from 1×10^8 parasites in TELT buffer (50 mM Tris-HCl, pH 8.0, 62.5 mM EDTA, 2.5 M LiCl, and 4% (v/v) Triton X-100) as described previously (12). The resulting 3.5-kb product was cloned into the PCR4Blunt-TOPO vector (Invitrogen) to generate the plasmid pTOPO-LFR1, and the correct coding sequence was confirmed by sequencing. The resulting amino acid sequence was used to find the predicted FAD and NADH binding pockets by conserved domain analysis (NCBI) (13, 14). The topology of the protein was modeled with the SOSUI algorithm (15), and the resulting predicted transmembrane topology was used to locate the two transmembrane helices containing the four invariant histidines. The protein sequences for *L. major LFR1* (LmLFR1, accession number XP_001684755), *A. thaliana FRO1* (AtFRO1, accession number NP_171665), *A. thaliana FRO2* (AtFRO2, accession number NP_171664), *Pisum sativum FRO1* (PsFRO1, accession number AAK95654), *Homo sapiens GP91-PHOX* (GP91-phox, accession number P04839), and *Saccharomyces cerevisiae FRE1* (ScFRE1, accession number NP_013315) were downloaded from the National Center for Biotechnology Information server and aligned with ClustalW (16). For *LFR1* ectopic expression, the *LFR1* ORF was cloned into the expression vector pXG-SAT (courtesy of S. Beverley, Washington University, St. Louis, MO) (17, 18). The *Leishmania* pXG vectors, developed by the Beverley laboratory, utilize the dihydrofolate reductase-thymidylate synthase 5′ and 3′ UTR regions to control transcription and reach ~10–20 copies per cell resulting in overexpression of cloned genes (18). The *LFR1* ORF was PCR-amplified with the primer set AFPNA13/AFPNA20, digested with BamHI enzyme, and cloned into a BamHI linearized pXG-SAT plasmid to generate pLFR1-SAT.

Gene Deletion Constructs—The gene deletion constructs LaKOLFR1Hyg and LaKOLFR1Neo, required for sequential deletion of both alleles of the *LFR1* gene, were based on the *Leishmania* expression vectors pXG-hyg and pXG-neo (courtesy of S. Beverly, (17)). A 1-kb flanking sequence upstream of the *L. amazonensis LFR1* ORF was amplified using a nested PRC strategy utilizing the outer primer set (AFPNA25/AFPNA36) followed by the nested primer set (AFPNA35/AFPNA37). A 600-bp flanking sequence downstream of the *L. amazonensis LFR1* ORF was amplified using a partial nested PCR strategy utilizing the outer primer set (AFPNA43/AFPNA38) followed by a second PCR using a primer set with one nested primer (AFPNA28/AFPNA43). The 5′- and 3′-flanking sequences were cloned into the pCR4-Blunt TOPO vector (Invitrogen) and sequenced to confirm the identity of the fragments. The 5′- and 3′-flanking regions were amplified with the primer sets AFPNA45/AFPNA46, encoding NruI and EcoRV restriction sites, and AFPNA47/AFPNA48, encoding EcoRV and HindIII restriction sites, and subsequently cloned into pCR4-Blunt TOPO vector creating the plasmids p5′-topo and p3′-topo. The 5′-flanking region was excised from the p5′-topo plasmid with SpeI and EcoRV enzymes and cloned into the p3′-topo plasmid linearized with the same enzymes to create the p5′3′-topo plasmid. To generate the deletion constructs, the spanning regions containing the DHFR-*Hyg* or (*Neo*)-TS were PCR-amplified from the pXG-based vectors with primers KO1 and KO2 and ligated into p5′3′-topo plasmid, linearized by EcoRV digestion. Plasmid DNA from each gene-targeted construct was digested with NruI and HindIII to release the integrating fragments, and the linearized gene deletion constructs were gel-purified.

Transfection and Generation of Δlfr1 L. amazonensis—Transfections of *L. amazonensis* promastigotes were performed as outlined in Huynh *et al.* (7). For generation of the Δ*lfr1* knock-out strain, the region containing the *LFR1* gene was replaced sequentially on both alleles by the hygromycin B phosphotransferase (*Hyg*) and neomycin phosphotransferase (*Neo*) genes, to confer resistance to the antibiotics hygromycin B and G418, respectively. 100 μg/ml hygromycin B and/or 50 μg/ml G418 were added to the medium used to expand the isolated colonies after each round of homologous gene targeting. Southern blots were performed to determine integration of the selectable markers at the *LFR1* locus. The digoxigenin-labeled probes for the *Hyg, Neo*, and *LFR1* genes were generated by PCR amplification with primer sets AFPNA57/AFPNA58, AFPNA62/AFPNA63, and AFPNA14/AFPNA17, respectively, according to the manufacturer's protocol (Roche Applied Science). Genomic DNA from candidate clones was isolated in TELT buffer as described previously (12) and digested with EcoRI/NotI (*Hyg*-probed bots), EcoRI/MfeI (*Neo*-probed blots), or MfeI/XhoI *(LFR1*-probed blots) enzymes overnight. The digests were run on a 1% agarose gel and transferred to nylon membranes. The blots were then blocked, hybridized, and probed with digoxigenin-labeled PCR probes according to the manufacturer's protocol (Roche Applied Science). The homozygous Δ*lfr1* strain was cultured in promastigote media supplemented with 100 μg/ml hygromycin B and 50 μg/ml G418. Complementation of Δ*lfr1* parasites with wild type *LFR1* was achieved by transfection of promastigotes with the episomal vector pLFR1-SAT. Agar-grown clones resistant to 50 μg/ml nourseothricin were selected for further characterization.

Quantification of LFR1 Transcripts by Quantitative PCR—The effect of iron deprivation on the *LFR1* transcript levels was ascertained by quantitative real time PCR analysis (qPCR). Log phase wild type *L. amazonensis* promastigotes were washed

twice in PBS, resuspended at 1×10^6 parasites per ml in promastigote medium lacking hemin, and incubated for 15 h at 26 °C. A total of 1×10^8 parasites was collected, and total RNA was isolated from three independent samples using Qiagen RNeasy kit (Qiagen) according to the manufacturer's protocol. cDNA synthesis was carried out using 1 μg of total RNA and qScript cDNA SuperMix (Quanta Biosciences). To quantify the levels of specific mRNA transcripts in individual samples, 1 μl of the cDNA was amplified with gene-specific primers (*LFR1* Fv/*LFR1* Rv) and *L. amazonensis* ubiquitin hydrolase (UbiqH FD/UbiqH Rv) as a reference gene with PerfeCTa SYBR Green FastMix (Quanta Biosciences) following the manufacturer's protocol using a C1000 thermocycler with the CFX96 real time system (Bio-Rad). Three technical and three biological replicates of each reaction were performed; amplification efficiencies were validated, and expression for the *LFR1* gene was normalized to the mRNAs encoding ubiquitin hydrolase, which is known to be expressed constitutively in *Leishmania* (19, 20).

Parasite Growth Assays—For procyclic promastigotes, a late log phase culture of *L. amazonensis* was used to inoculate parasites at 1×10^5 parasites/ml in promastigote medium and incubated at 26 °C. For axenic amastigotes, a log phase culture of *L. amazonensis* was used to inoculate parasites at 1×10^5 parasites/ml in amastigote medium and incubated at 32 °C. A sample of the cultures was taken every 24 h and incubated with 5 μM fluorescein diacetate for 5 min. Fluorescent parasites were visualized with a Nikon Eclipse E200 microscope with a 40× NA 0.75 objective (Nikon) and counted on a bright line hemocytometer (Hausser Scientific). The data were analyzed for statistical significance using an unpaired Student's *t* test ($p < 0.05$ was considered significant).

Iron Reductase Assays—The ability of parasites to reduce extracellular ferric iron to ferrous iron was measured with the cell-impermeable compound potassium hexacyanoferrate ($K_3Fe(CN)_6$) as described previously (9, 21). Briefly, log phase promastigotes or axenic amastigotes were washed twice in PBS, resuspended at 1×10^6 parasites per ml in promastigote or amastigote media lacking or supplemented with hemin, and incubated for 15 h at 26 °C for promastigotes and 32 °C for amastigotes. The parasites were harvested by centrifugation, washed twice in PBS, and either 1×10^8 or 3×10^7 parasites were resuspended in 1 ml of HBSS containing 1 mM $K_3Fe(CN)_6$. The reduction of the ferric to ferrous form of $K_3Fe(CN)_6$ was monitored by the change in absorbance at 420 nm. Samples (50 μl) were taken every hour, centrifuged at 10,000 × *g* for 5 min, and read on a SpectraMax 5e plate reader (Molecular Devices). A standard curve of $K_3Fe(CN)_6$ was used to convert A_{420} readings into millimolar $K_3Fe(CN)_6$. Data were plotted with Microsoft Excel (Microsoft) and line-fitted to determine rates of Fe^{3+} reduction.

Field Emission Scanning Electron Microscopy—Log phase promastigotes, 7-day stationary phase metacyclic, or axenic amastigotes were attached to poly-L-lysine-coated glass coverslips and fixed for 2 h in 2% glutaraldehyde, 2% paraformaldehyde, 0.1 M HEPES, pH 7.0, at room temperature. Samples were then post-fixed in 1% OsO_4 in 0.1 M HEPES, pH 7.4, for 1 h and then exposed to 1% tannic acid (in water) for 1 h before dehydration in an ethanol series, critical point dried from CO_2, and gold-sputtered (22). Images were acquired on a Hitachi S-4800 field emission scanning electron microscope operated at 5 kV. All reagents were obtained from Electron Microscopy Sciences.

Live Microscopy—To determine the percentage of live and dead parasites, samples were taken 48 h after transfer to amastigote media at 32 °C and incubated with 5 μM fluorescein diacetate, to detect living parasites (green fluorescence), and 150 μM propidium iodide, to detect dead parasites (red fluorescence), for 5 min at room temperature. Parasites were transferred to a bright line hemocytometer and counted on a Nikon Eclipse E200 microscope with a ×40 NA 0.75 objective (Nikon). To determine the percentage of motile *versus* nonmotile parasites, samples of axenic amastigotes were taken at 48 h post-induction and observed via phase contrast microscopy on a Nikon Eclipse E200 microscope with a ×40 NA 0.75 objective. Parasites were scored as motile if movement of the parasite or flagellar beating was observed. Parasites failing to meet the former criteria were scored as nonmotile. To determine parasite length, 48 h post-induction axenic amastigotes or 7-day stationary phase metacyclic promastigotes were imaged by differential interference contrast microscopy on a Nikon Eclipse Ti inverted microscope with a ×100 NA 1.4 objective (Nikon) equipped with a Hamamatsu C9100-50 camera. Acquired images were analyzed with the Volocity software suite (PerkinElmer Life Sciences).

Immunofluorescence Microscopy—48 h post-induction, axenic amastigotes or mid-log phase promastigotes were harvested, washed three times in PBS, and fixed with 4% paraformaldehyde. The fixed parasites were permeabilized with 0.05% Triton X-100, washed in PBS, and adhered to poly-L-lysine-coated coverslips. The samples were blocked with 5% horse serum in PBS for 1 h, and incubated with mouse monoclonal antibodies against the P4 antigen (23) (courtesy of D. McMahon-Pratt, Yale University, New Haven, CT) for 1 h at room temperature. After incubation, the coverslips were washed three times with PBS and incubated with Texas Red-conjugated goat anti-mouse antibodies (Invitrogen) for 1 h at room temperature. The coverslips were then washed three times with PBS, incubated with 36 μM DAPI, washed with PBS, and mounted in ProLong mounting media (Invitrogen) prior to imaging on a Leica TCS SP5 X Supercontinuum confocal microscope using a ×63 NA 1.2 objective. Image acquisition was performed with the Leica application suite software package. Image analysis was performed with the Volocity software suite.

Infection of Primary Bone Marrow Macrophages—Bone marrow-derived macrophages from BALB/c mice (NCIS) were prepared as described previously (24), seeded onto 24-well plates containing coverslips at a density of 7×10^4 cells per well, and incubated overnight in BMM[2] media (RPMI 1640 medium supplemented with 10% FBS and 5% L cell supernatant (as a source of M-CSF)) at 37 °C and 5% CO_2. Adherent macrophages were washed with fresh RPMI 1640 medium and infected with axenic amastigotes in 0.5 ml of RPMI 1640 medium supplemented with 5% FBS (multiplicity of infection = 1.0 or 1.5). After 1 h at 34 °C and 5% CO_2, free parasites were removed by three washes

[2] The abbreviation used is: BMM, bone marrow-derived macrophage.

with PBS and further incubated for various amounts of time in RPMI 1640 medium supplemented with 10% FBS and 5% L cell supernatant at 34 °C and 5% CO_2.

For rescue experiments with cationic ferritin, macrophages were isolated and plated as outlined above. One hour before infection, BMM media were replaced with fresh BMM media supplemented with 10 μg/ml cationized ferritin from horse spleen (Sigma). Adherent macrophages were washed with fresh RPMI 1640 medium and infected with axenic amastigotes in 0.5 ml of RPMI 1640 medium supplemented with 5% FBS (multiplicity of infection = 1.0). After 1 h at 34 °C and 5% CO_2, cultures were washed with PBS to remove extracellular parasites and further incubated for various amounts of time in BMM media supplemented with 10 μg/ml cationized ferritin.

Coverslips were fixed after 1 h (zero hour time point) and 24, 48, and 72 h of incubation with 2% paraformaldehyde, permeabilized with 0.02% Triton X-100, and stained with 35 μM DAPI. The number of intracellular parasites (identified through the characteristic kinetoplast DNA staining pattern with DAPI and localization within parasitophorous vacuoles by phase contrast) was quantified on a Nikon Eclipse E200 microscope with a ×100 NA 1.4 objective (Nikon) in a minimum of 400 macrophages per coverslip, in triplicate. The data were expressed as the total number of intracellular parasites per 100 macrophages. The data were analyzed for statistical significance using an unpaired Student's *t* test ($p < 0.01$ was considered significant). Images of the infected macrophages were taken with a Nikon DS-Fi1 camera and processed with the Volocity software suite.

In Vivo Virulence and Persistence Assays—Female BALB/c mice were injected in the right hind footpad with 1.0×10^6 mAb 3A.1-purified metacyclic promastigotes of *L. amazonensis* (10, 11), and lesion progression was followed by blinded weekly measurements with a caliper. The parasite tissue load of wild type and Δ*lfr1 L. amazonensis* was determined after 9 or 11 weeks, respectively, using a limiting dilution assay (7, 25). Promastigotes derived from parasites isolated from footpad lesions were transferred to amastigote axenic media and subsequently used for infections in BMM. Statistical significance between means of the two groups was determined using a two-tailed Student's *t* test for independent samples.

RESULTS

Leishmania LFR1 Gene Encodes a Membrane Protein with Ferric Reductase Activity That Is Induced by Iron Deficiency—Homology searches of the *L. major* data base identified LmjF30.1610, a gene on chromosome 30 (GenBank™ accession number XP_001684755) with 36% identity and 45% similarity to *FRO1*, the ferric reduction oxidase gene from *Arabidopsis thaliana*. PCR amplification and cloning of the corresponding 3.5-kb *LFR1* from genomic DNA of *L. amazonensis* (the species responsible for cutaneous leishmaniasis in the New World) revealed extensive identity with the *L. major* sequence (supplemental Fig. S1). *LFR1* contains the PFAM ferric reductase-like transmembrane component (Ferric_reduct (PF01794)) found in other NADPH-dependent oxidoreductases (*A. thaliana* FRO1 and FRO2; *S. cerevisiae* FRE1 and FRE2; *Schizosaccharomyces pombe* FRP1; and *H. sapiens* GP91-phox), along with the ferric reductase NAD binding domain (NAD_binding_6 (PF08030)) and the FAD binding domain (FAD_binding_8 (PF08022)), which together promote transmembrane electron transfer (26). Specifically, LFR1 contains the highly conserved residues HPFT in the FAD-binding motif, the residues GPyG in the NAD-binding motif, and the four invariant transmembrane histidines that are found in *A. thaliana* FRO1 and FRO2, *P. sativum* FRO1, and *S. cerevisiae* FRE1 (supplemental Fig. S2) (27–29).

The *LFR1* gene encodes a 1084-amino acid protein with a calculated molecular mass of 119 kDa. Hydropathy analysis predicts 11 transmembrane domains, including an apparent N-terminal signal peptide. The C-terminal region containing the FAD- and NADPH-binding sites is predicted to be in contact with the cytosol. Four conserved histidines likely to mediate heme binding (29, 30) are present in transmembrane domains 9 (residues His-458 and His-472) and 11 (residues His-542 and His-556) (Fig. 1*A* and supplemental Fig. S1).

The sequence similarity with *Arabidopsis FRO1* and the presence of functionally conserved motifs suggested that *LFR1* encodes a plasma membrane ferric reductase. To directly test this hypothesis, we performed ferric reductase activity assays utilizing the membrane-impermeable compound, hexacyanoferrate, as a means to monitor the ferric reductase activity present on the surface of live promastigote forms of the parasites. Consistent with the high levels of sequence identity between *LFR1* from *L. amazonensis* and the corresponding genes in *L. major* (causative agent of cutaneous leishmaniasis in the Old World) (supplemental Fig. S1), live promastigotes from five distinct *Leishmania* isolates were able to reduce extracellular ferric iron. Higher levels of reductase activity were observed associated with species that cause cutaneous lesions (*L. major*, 1.40 ± 0.29 fmol of hexacyanoferrate/h/cell; *L. amazonensis*, 1.27 ± 0.18 fmol of hexacyanoferrate/h/cell), when compared with species that cause visceral disease (*L. donovani*, 0.55 ± 0.16 fmol of hexacyanoferrate/h/cell; *L. chagasi,* 0.47 ± 0.09 fmol of hexacyanoferrate/h/cell; and *L. infantum*, 0.49 ± 0.03 fmol of hexacyanoferrate/h/cell) (Fig. 1*B*).

To demonstrate that *LFR1* directly confers ferric reductase activity to *Leishmania*, *L. amazonensis* promastigotes were transfected with the *LFR1* overexpressing vector, pLFR1-SAT, or vector alone. Parasites transfected with pLFR1-SAT showed a 3-fold increase in ferric reductase activity levels (from 1.37 ± 0.09 fmol of hexacyanoferrate/h/cell to 4.39 ± 0.44 fmol of hexacyanoferrate/h/cell) (Fig. 1*C*). These assays were performed with promastigotes incubated for 15 h in media lacking the major source of iron, hemin, because several previously described reductases are induced by iron deficiency (4, 5). As predicted, *LFR1* transcript levels were >3-fold higher in *L. amazonensis* promastigotes incubated in iron-deficient media, when compared with parasites kept in the presence of hemin (Fig. 2*A*). In addition, the reductase activity of the parasites grown in iron-deficient media was increased by 27% (from 0.87 ± 0.10 fmol to 1.19 ± 0.16 fmol of hexacyanoferrate/h/cell) when compared with parasites grown in the presence of hemin (Fig. 2*B*).

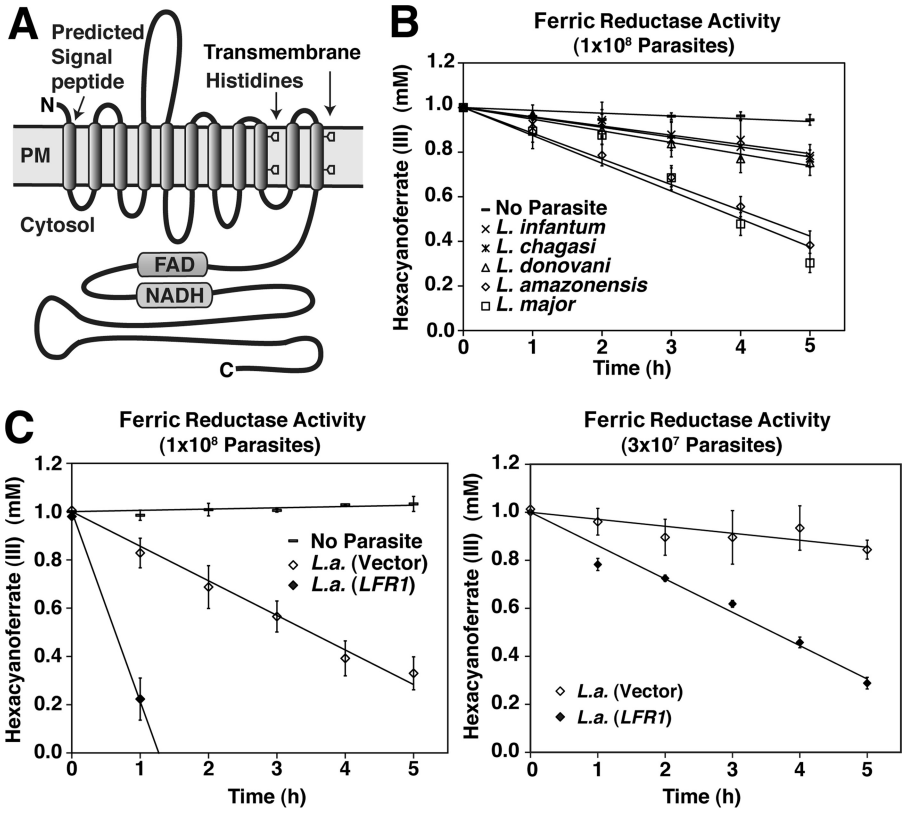

FIGURE 1. ***Leishmania LFR1* gene encodes a membrane protein with ferric reductase activity.** *A,* model of the predicted membrane topology of *Leishmania* ferric reductase 1 (LFR1) highlighting the transmembrane histidines, FAD, and NADH motifs present in ferric reductases. *B,* five isolates of *Leishmania* (*L. infantum*; *L. chagasi*; *L. donovani*; *L. amazonensis*; and *L. major*) were assayed for ferric reductase activity. Parasites were grown to mid-log phase, transferred to promastigote media lacking hemin for 15 h, washed, and resuspended in assay buffer at 1×10^8 parasites/ml, and ferric reductase activity was monitored spectrophotometrically. All five strains of *Leishmania* assayed showed ferric reductase activity, whereas no activity was detectable in assay buffer alone (——). *C, L. amazonensis* parasites were transfected with an *LFR1* overexpression vector, pLFR1-SAT or vector alone, and 1×10^8 (*left graph*) or 3×10^7 (*right graph*) parasites/ml were assayed for ferric reductase activity. The data represent the mean ± S.D. of triplicate determinations and are representative of at least four independent experiments.

LFR1 Is the Major Surface Ferric Reductase of L. amazonensis Promastigotes—Two sequential rounds of transfection of *L. amazonensis* promastigotes with *LFR1* gene deletion constructs followed by drug selection were used to generate heterozygote (*LFR1*/Δ*lfr1*) and homozygote null (Δ*lfr1*/Δ*lfr1*) clones (Fig. 3*A*). No growth defects in complete promastigote culture media were observed between wild type (*LFR1/LFR1*) and *LFR1* null (Δ*lfr1*/Δ*lfr1*) promastigotes (Fig. 3*C*), allowing expansion of the null strain. Ferric reductase activity was reduced in *LFR1*/Δ*lfr1* consistent with a single copy gene deletion and undetectable in null Δ*lfr1*/Δ*lfr1* parasites. The ferric reductase activity, calculated from the linear slope fitted to the data, was as follows: *LFR1/LFR1,* 1.68 ± 0.17 fmol of hexacyanoferrate/h/cell; *LFR1*/Δ*lfr1,* 0.49 ± 0.13 mM fmol of hexacyanoferrate/h/cell; and Δ*lfr1*/Δ*lfr1,* not detectable (Fig. 3*B*). This result demonstrates that *LFR1* encodes the major ferric reductase protein exposed on the surface of *Leishmania* promastigotes. LFR1 is thus likely to be the major enzyme responsible for the conversion of Fe^{3+} into Fe^{2+} for intracellular transport by the *Leishmania* membrane transporter LIT1 (6, 7).

LFR1-deficient L. amazonensis Promastigotes Are Defective in Differentiation into Infective Metacyclic and Amastigote Forms—Wild type and *LFR1* null (Δ*lfr1*) *L. amazonensis* promastigotes were grown to stationary phase, a condition that induces differentiation to metacyclic promastigote forms capable of initiating infections in mammalian hosts (31). The expected number of metacyclic promastigotes was isolated from cultures of wild type *L. amazonensis*. In contrast, there was a 5-fold reduction in the number of metacyclic promastigotes (defined as not being agglutinated by the 3A.1 mAb) isolated from Δ*lfr1 L. amazonensis* cultures (Fig. 4*A*).

Scanning electron microscopy examination showed that wild type and Δ*lfr1* parasites present in mid-log phase had a normal morphology, typical of replicating promastigote forms. However, examination of stationary phase cultures revealed striking morphological alterations in the Δ*lfr1* strain. Although most wild type parasites from the stationary phase cultures had the elongated cylindrical morphology typical of this life cycle stage, Δ*lfr1* parasites showed a very heterogeneous morphology, ranging from long cylindrical forms resembling normal metacyclic forms to bulbous forms displaying long flagella (Fig. 4*B*). To quantify this phenotype, wild type parasites transfected with vector alone and Δ*lfr1* parasites transfected with pLFR1-SAT or vector alone were grown to stationary phase and subjected to microscopic imaging and long axis cell body measurements. Wild type parasites transfected with vector alone displayed elongated forms with the majority of the cell bodies ranging from 7 to 12 μm in length, whereas Δ*lfr1* parasites transfected with vector alone had a heterogeneous distribution of cell body length, ranging from 4 to 14 μm. The Δ*lfr1* promastigotes

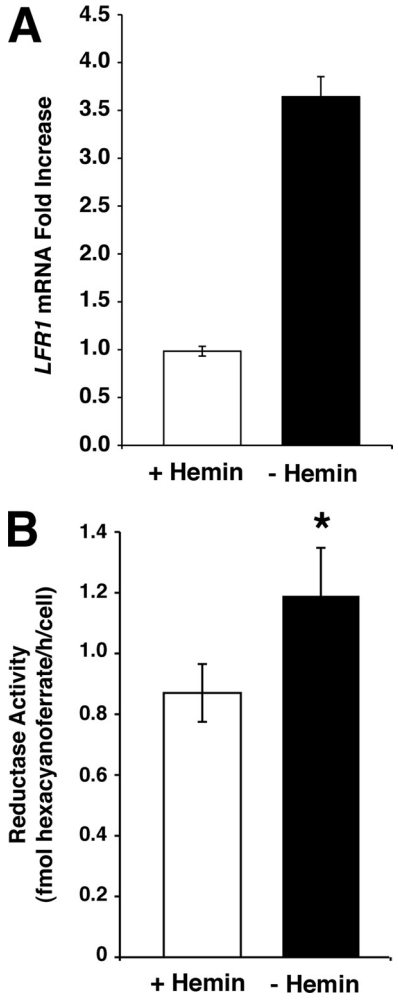

FIGURE 2. ***LFR1* transcript levels increase in response to iron deprivation.** *L. amazonensis* promastigotes were grown to mid-log phase at 26 °C, washed, and transferred to complete promastigote medium containing hemin (*white columns*) or medium lacking hemin (*black columns*) for 15 h at 26 °C. *A,* total of 1×10^8 parasites were collected; total RNA was isolated, and transcript levels were quantified by quantitative PCR. The data represent the mean ± S.D. of triplicate determinations and are representative of three independent experiments. *LRF1* transcript levels from parasites grown in media lacking hemin were increased 2.5-fold when compared with parasites grown in complete media. *B,* after 15 h of incubation in the presence or absence of hemin, the parasites were resuspended in assay buffer at 1×10^8 parasites/ml, and ferric reductase activity was monitored spectrophotometrically. Parasites grown without hemin had a significant increase in reductase activity, when compared with parasites grown in complete hemin-containing media (Student's *t* test, $p < 0.01$). The data represent the mean ± S.D. of triplicate determinations and are representative of three independent experiments.

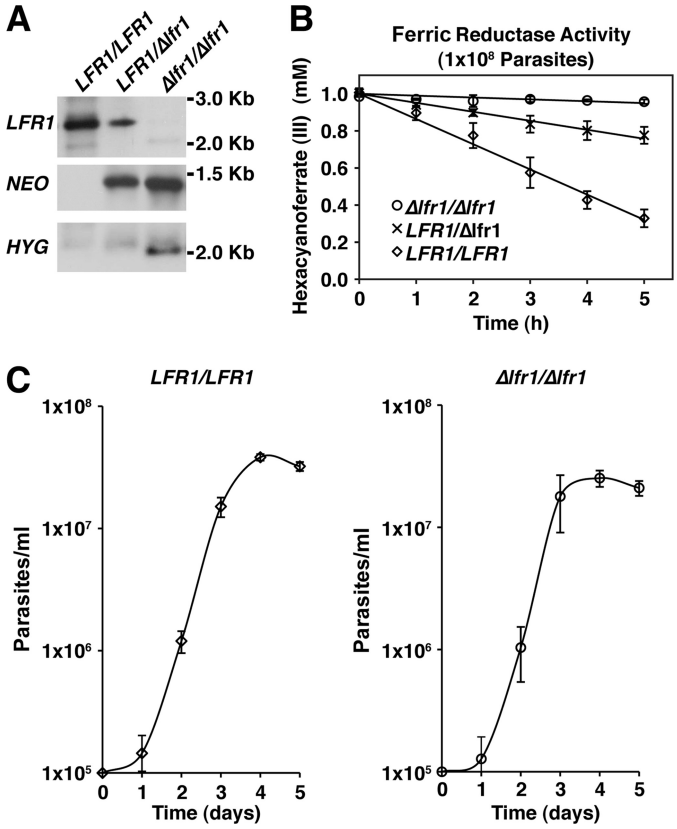

FIGURE 3. ***LFR1* is responsible for the observed ferric reductase activity but is not required for normal promastigote growth.** Generation and characterization of *LFR1* null mutants. *A,* Southern blots of genomic DNA from wild type (*LFR1/LFR1*), heterozygous mutant (*LFR1/*Δ*lfr1*), and homozygous null mutant (Δ*lfr1/*Δ*lfr1*) promastigotes digested with restriction enzymes and probed for *Neo, Hyg, or LFR1* ORFs. The sequential replacement of the *LFR1* gene is indicated by the *LFR1*-containing 2.5-kb fragment in lanes representing wild type and heterozygous parasites, a *Neo*-containing 1.5-kb fragment in lanes representing heterozygous and homozygous *LFR1* null parasites, and a *Hyg*-containing 2-kb fragment in lanes representing homozygous *LFR1* null parasites. *B,* ferric reductase activity of wild type (*LFR1/LFR1,* ◇), heterozygous (*LFR1/*Δ*lfr1,* ×), or homozygous *LFR1* null (Δ*lfr1/*Δ*lfr1,* ○) parasites. Promastigotes were grown to mid-log phase, transferred to promastigote media lacking hemin for 15 h, and washed, and 1×10^8 parasites/ml were assayed for ferric reductase activity. The data represent the mean ± S.D. of triplicate determinations and are representative of at least five independent experiments. *C,* growth curves of wild type (*LFR1/LFR1*) and *LFR1* null (Δ*lfr1/*Δ*lfr1*) promastigotes in liquid culture. There were no significant differences in promastigote growth rates between the two strains.

transfected with pLFR1-SAT displayed a partially restored morphology, as determined by long axis cell body measurements. However, although the number of elongated cylindrical forms typical of metacyclic promastigotes was increased, numerous shorter and bulbous forms were still present (Fig. 4*C*). Transfection of wild type and Δ*lfr1* promastigotes with the empty pXG-SAT vector did not alter the metacyclic form morphology observed in the absence of transfection (data not shown).

Next, we investigated whether LFR1 was required for the generation of amastigotes, the rounded nonmotile *Leishmania* life cycle stages that replicate within host macrophages. In *L. amazonensis,* promastigotes can be induced to differentiate into axenic amastigotes by shifting the parasites to culture medium that resembles the intracellular conditions of low pH (pH 4.5) and elevated temperature (32 °C) (32). When this procedure was performed in parallel with wild type and Δ*lfr1* promastigotes, wild type parasites differentiated normally and replicated as axenic amastigotes. In contrast, no detectable growth as amastigotes was observed with Δ*lfr1* parasites (Fig. 5*A*). After 48 h of incubation in amastigote medium, 95% of wild type parasites had assumed the rounded amastigote morphology and were no longer motile, whereas only 60% of Δ*lfr1* parasites were nonmotile (Fig. 5*B*). The viability of Δ*lfr1* parasites was also reduced under these conditions, as determined with a fluorescent live/dead assay (Fig. 5*C*). Scanning electron microscopy analysis of the morphology of parasites after 48 h in amastigote culture conditions showed that the recently differentiated wild type amastigotes had the expected rounded and

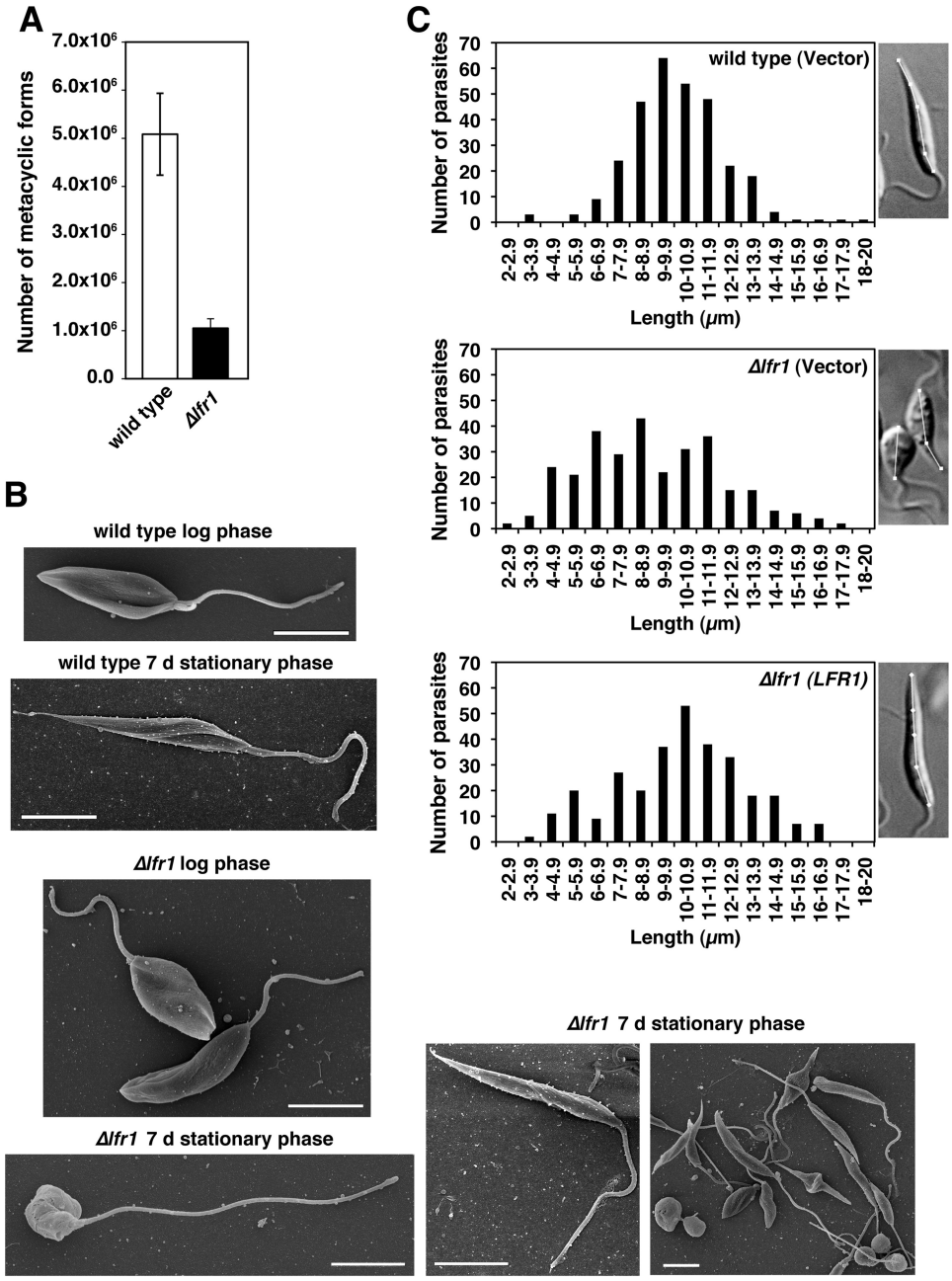

FIGURE 4. ***LFR1* null *L. amazonensis* is defective in differentiation into infective metacyclic forms.** *A,* total of 1×10^8 parasites were used to isolate metacyclic forms from 7-day stationary phase promastigote cultures by preferential agglutination of promastigotes with the 3A.1 mAb. The data represent the mean number of metacyclic forms recovered ± S.D. of triplicate determinations and are representative of three independent experiments. *B,* parasites from mid-log or stationary phase cultures were adhered to polylysine-coated coverslips and processed for scanning electron microscopy. Images show representative morphological forms for each condition. Quantification of a total of 140 Δ*lfr1* parasites revealed three main morphological forms: long cylindrical (35%), long bulbous (31%), or short bulbous (34%). *Scale bars,* 5 μm. *C,* wild type and Δ*lfr1* parasites were transfected with empty pXG-SAT vector (wild type (*vector*) and Δ*lfr1* (*vector*)) or pLFR1-SAT (Δ*lfr1* (*LFR1*)) and grown to stationary phase. Parasites from each strain were imaged by differential interference contrast microscopy, and the longest cell body axis was measured as indicated with the *white lines* in the *insets*. Wild type length = 12.0 μm, Δ*lfr1* (*vector*) = 5.0 and 8.5 μm, and Δ*lfr1* (*LFR1*) = 13.5 μm. A total of 300 parasites was measured for each strain.

compact cell shape, whereas Δ*lfr1* parasites showed a more heterogeneous morphology, with different degrees of incomplete shortening of the cell body and flagella (Fig. 5*D*). Despite the observed differences in morphological differentiation, both wild type and Δ*lfr1 L. amazonensis* expressed the amastigote marker P4 (23) when promastigote cultures were shifted to amastigote growth medium (Fig. 5*E*). These findings suggest that in the absence of LFR1 the differentiation process into amastigotes is initiated but is not completed.

Transfection with pLFR1-SAT, followed by a shift to amastigote medium at 32 °C and pH 4.5, resulted in increased ferric reductase activity, from 0.71 ± 0.10 to 4.32 ± 0.60 fmol of hexacyanoferrate/h/cell in wild type and from undetectable levels to 1.98 ± 0.08 fmol of hexacyanoferrate/h/cell in Δ*lfr1* promastigotes (Fig. 6*A*). The increase in *LFR1* expression did not rescue the inability of Δ*lfr1* to grow as axenic amastigotes (Fig. 6*B*). Notably, *LFR1* overexpression markedly inhibited the growth of wild type axenic amastigotes, suggesting a toxic effect

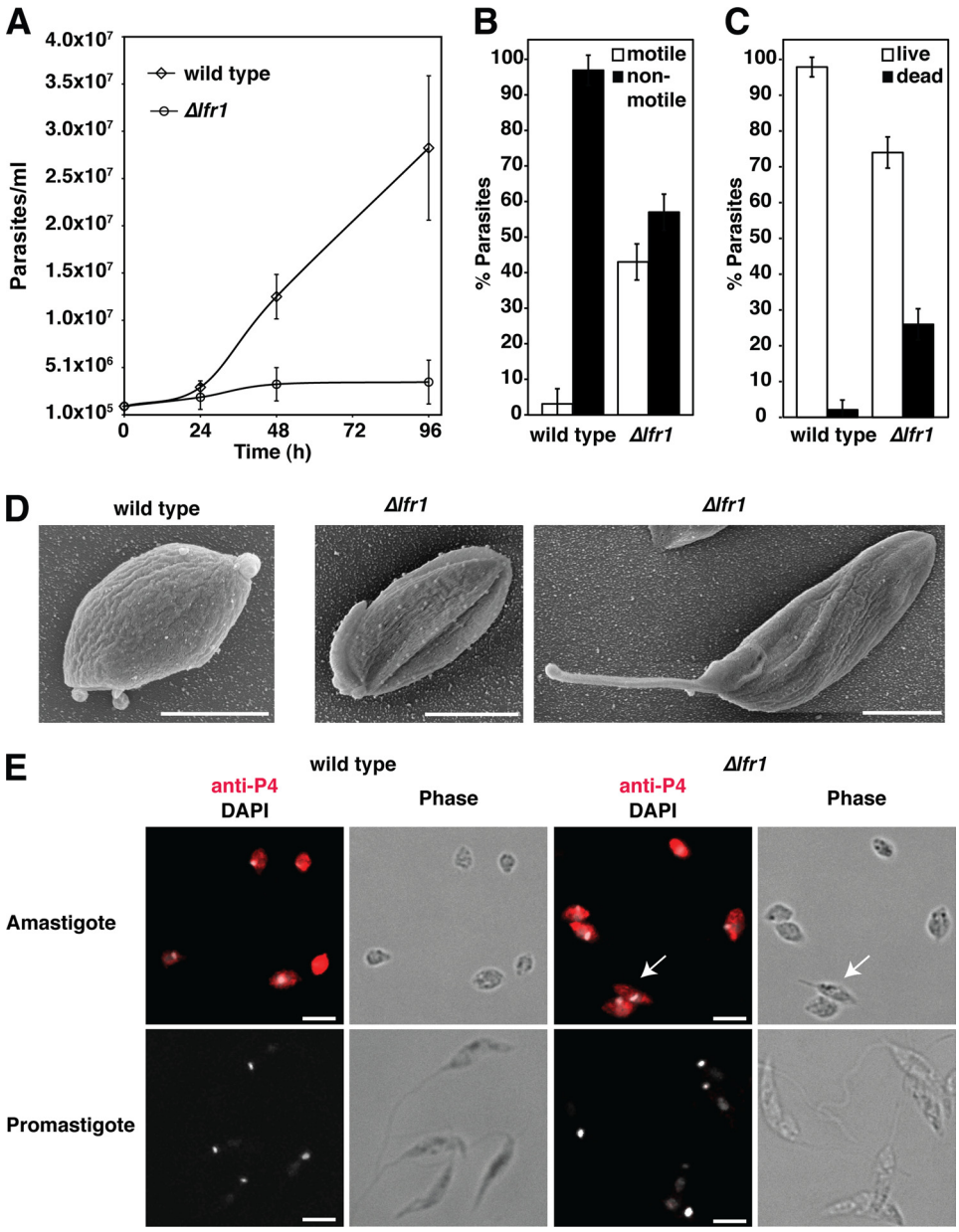

FIGURE 5. ***LFR1* null *L. amazonensis* is defective in differentiation into axenic amastigotes.** Mid-log phase wild type or *LFR1* null promastigotes (Δ*lfr1*) were washed, resuspended in pH 4.5 amastigote growth media at 1×10^5 parasites/ml, and cultured at 32 °C. *A,* growth curves of wild type (◇) and Δ*lfr1* parasites (○). The data represent the mean ± S.D. of triplicate determinations and are representative of four independent experiments. *B–D,* wild type and Δ*lfr1 L. amazonensis* 48 h after switching to amastigote media. *B,* parasite motility was assayed by live phase microscopy. The percentages of motile (*white columns*) or nonmotile (*black columns*) parasites for wild type or Δ*lfr1* are shown. The data represent the mean ± S.D. of quadruplicate determinations. *C,* viability was assessed by parasite treatment with 5 μM fluorescein diacetate (green) and 150 μM propidium iodide (red) followed by live fluorescence imaging. *Green cells* were scored as "live" (*white columns*), and red cells were scored as "dead" (*black columns*). The data represent the mean ± S.D. of quadruplicate determinations. *D,* samples of wild type and Δ*lfr1* amastigote cultures were adhered to polylysine-coated coverslips and processed for scanning electron microscopy. *Scale bars,* 5 μm. *E,* samples were taken from wild type and Δ*lfr1* mid-log cultures or 48-h axenic amastigote cultures, fixed, permeabilized, and stained by immunofluorescence with antibodies against the amastigote-specific antigen P4 (*red*) and the nuclear stain DAPI (*gray*). The *white arrows* indicate an incompletely differentiated Δ*lfr1* parasite displaying P4 staining. *Scale bars,* 5 μm.

(Fig. 6*B*). Viability assays confirmed an increase in the number of dead parasites after LFR1 overexpression, in both wild type and Δ*lfr1* parasites (Fig. 6*C*). Imaging followed by cell body length measurements revealed that LFR1 expression in Δ*lfr1* parasites only partially restored the morphological shift from the elongated promastigote shape to the shortened round amastigotes (Fig. 6*D*). To determine the infectivity of these forms, parasites transfected with pXG-SAT alone or pLFR1-SAT were incubated for 48 h in amastigote medium, and infection of BMM was performed. In agreement with their inability to replicate as axenic amastigotes, Δ*lfr1* parasites did not replicate within macrophage phagolysosomes. In contrast, wild type parasites expressing the empty vector showed vigorous intracellular replication, confirming that transfection alone did not reduce parasite viability. The inhibition in intracellular growth was also not due to an attenuation caused by extended culturing, as Δ*lfr1* parasites freshly isolated from mice displayed the same phenotype (supplemental Fig. S3). A strong inhibition in

the intracellular replication of both wild type and Δ*lfr1* parasites was observed when *LFR1* was overexpressed, consistent with the toxic effect of high levels of LFR1 (Fig. 6*E*).

To determine whether the inability of Δ*lfr1* amastigotes to replicate within cultured BMM also occurred *in vivo*, wild type and Δ*lfr1* metacyclic promastigotes were inoculated into the footpads of BALB/c mice. As shown in Fig. 4*A*, despite the reduction in number, metacyclic parasites could be purified from the mixed morphology 7-day stationary phase cultures of Δ*lfr1*. As expected, a progressive growth in the size of cutane-

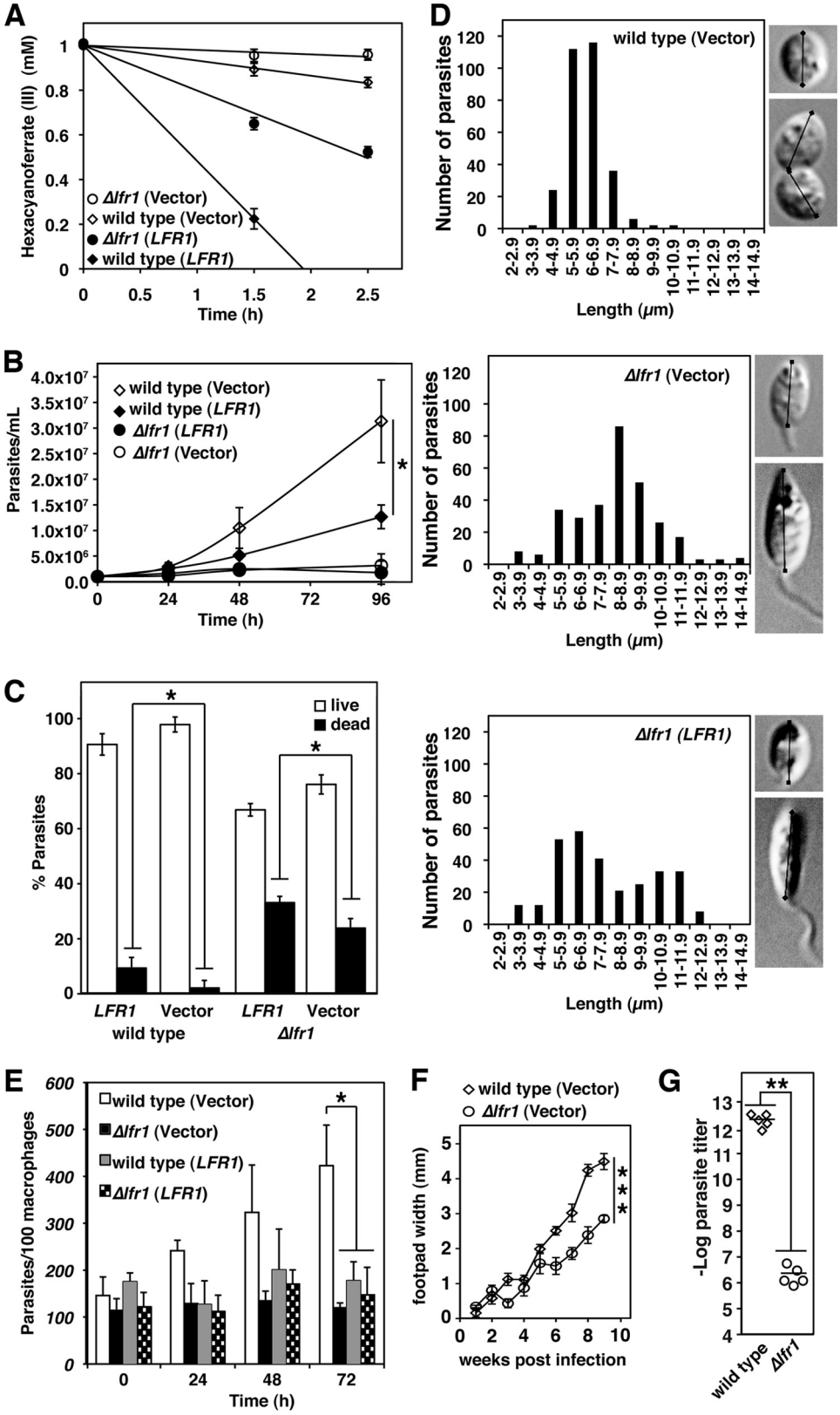

ous lesions was observed in mice injected with wild type *L. amazonensis* metacyclic promastigotes. In contrast, lesion development was significantly delayed in mice inoculated with Δ*lfr1* metacyclic promastigotes (Fig. 6*F*). Because lesion development measurements based on footpad swelling reflect inflammation and not the absolute number of parasites in the tissue, quantification of parasite load in the mouse footpads was also performed using a limiting dilution assay (33). The average number of Δ*lfr1* parasites per footpad was reduced by a factor of 10^6 when compared with wild type parasites (Fig. 6*G*), demonstrating their impaired virulence.

LFR1 Overexpression Inhibits Growth of Wild Type L. amazonensis Amastigotes but Rescues Replication of Amastigotes Lacking the Fe^{2+} Transporter LIT1—The results discussed above indicate that LFR1 is required for the transformation of *L. amazonensis* promastigotes into amastigotes, and for their sustained axenic growth. Overexpression of *LFR1* was found to have toxic effects on the parasites, precluding a rescue of the metacyclic and amastigote differentiation defects. This finding was not totally unexpected, because it is known that cells have to exert tight control over the levels of cellular Fe^{2+}, to avoid the generation of toxic radicals in aerobic environments (3). To test the hypothesis that the toxicity caused by overexpression of LFR1 is a result of excessive production and uptake of Fe^{2+}, we overexpressed *LFR1* in Δ*lit1,* an *L. amazonensis* null mutant lacking the Fe^{2+} iron transporter LIT1 (7).

Reflecting the endogenous levels of LFR1, wild type and Δ*lit1* promastigotes transfected with pXG-SAT alone had similar levels of ferric reductase activity (wild type (vector) = 1.01 ± 0.09 fmol of hexacyanoferrate/h/cell; Δ*lit1* (vector) = 1.03 ± 0.09 fmol of hexacyanoferrate/h/cell), and Δ*lit1* promastigotes transfected with pLFR1-SAT showed the expected activity increase (Δ*lit1* (*LFR1*) = 4.66 ± 0.90 fmol of hexacyanoferrate/h/cell) (Fig. 7*A*). This pattern of expression was maintained when the transfected promastigotes were induced to differentiate into axenic amastigotes at pH 4.5 at 32 °C (wild type (vector) = 0.63 ± 0.15 fmol of hexacyanoferrate/h/cell; Δ*lit1* (vector) = 0.90 ± 0.14 fmol of hexacyanoferrate/h/cell; Δ*lit1* (*LFR1*) = 3.38 ± 0.05 fmol of hexacyanoferrate/h/cell) (Fig. 7*B*). When the rate of growth of these transfected parasites as axenic amastigotes was determined, we observed a reduction in Δ*lit1* replication when compared with wild type parasites, which is consistent with the data presented above and with the results of previous studies (7). Remarkably, overexpression of *LFR1* in Δ*lit1* did not result in the toxic effects observed in wild type *L. amazonensis* (Fig. 6*B*), allowing vigorous amastigote replication and a full rescue of the Δ*lit1* growth defect (Fig. 7*C*).

Previous studies revealed that Δ*lit1* amastigotes were unable to replicate in BMM (7). To test if overexpression of LFR1 rescued the growth of intracellular amastigotes, wild type and Δ*lit1* parasites transfected with pXG-SAT alone or pLFR1-SAT were used to infect BMM. As reported previously, the number of intracellular Δ*lit1* amastigotes decreased over time (7). In contrast, overexpression of *LFR1* led to a significant increase in the numbers of intracellular amastigotes, when compared with Δ*lit1* parasites transfected with vector alone (Fig. 7*D*). Thus, the toxic effects of LFR1 overexpression on axenic or intracellular amastigotes require expression of the Fe^{2+} iron transporter LIT1.

LFR1-deficient Parasites Are Able to Replicate within Macrophages Loaded with an Exogenous Source of Iron—Cationic ferritin binds to negative charges on the plasma membrane, is endocytosed, concentrated in lysosomes, and degraded releasing Fe^{3+} for transport to the cytoplasm (34, 35). Because Δ*lfr1* parasites retain a functional LIT1 transporter that promotes ferrous iron acquisition by amastigotes within phagolysosomes (7), we hypothesized that loading the lysosomal compartment of macrophages with excess exogenous iron should be able to promote the replication in Δ*lfr1* amastigotes. To test this hypothesis, BMM were incubated in BMM medium alone or BMM medium supplemented with 10 μg/ml cationic ferritin for 1 h, followed by infection with wild type, Δ*lfr1,* and Δ*lit1* parasites. As expected, Δ*lfr1* and Δ*lit1* parasites failed to replicate in BMM grown in regular BMM medium, whereas the number of wild type parasites increased progressively between 24 and 72 h after infection (Fig. 8, *A* and *B*). However, in BMM preincubated with cationic ferritin, wild type, Δ*lfr1*, and Δ*lit1* parasites all displayed progressive intracellular growth and formed the typically enlarged parasitophorous vacuoles containing multiple amastigotes (Fig. 8, *A* and *B*).

FIGURE 6. ***LFR1* null *L. amazonensis* has a strong growth defect as axenic amastigotes and has reduced virulence.** *LFR1* overexpression partially rescues the defective differentiation defect of *LFR1* null *L. amazonensis* but impairs viability and replication of wild type and *LFR1* null parasites. Wild type and Δ*lfr1* promastigotes were transfected with the pXG-SAT vector alone (*vector*) or pLFR1-SAT (*LFR1*). Mid-log phase promastigotes were resuspended in amastigote growth media at 1×10^5 parasites/ml and cultured at 32 °C. *A,* ferric reductase activity of axenic amastigotes after 48 h in amastigote media. Wild type (◆) and Δ*lfr1* (●) parasites transfected with pLFR-SAT1 have higher ferric reductase activity than wild type (◇) or Δ*lfr1* (○) transfected with vector alone. The data represent the mean ± S.D. of triplicate determinations. *B,* growth curves of wild type and Δ*lfr1* parasites transfected with vector alone (*vector*) or pLFR1-SAT (*LFR1*). The data represent the mean ± S.D. of quadruplicate determinations. The *asterisk* indicates significant differences between wild type (*vector*) and wild type (*LFR1*) (Student's *t* test, $p < 0.02$). *C,* parasite viability was determined 48 h after switching to amastigote media by incubation with 5 μM fluorescein diacetate (green) and 150 μM propidium iodide (red). Green fluorescent parasites were scored as live, and red fluorescent parasites were scored as dead. The data represent the mean ± S.D. of quadruplicate determinations. The *asterisk* indicates significant differences between wild type (*vector*) and wild type (*LFR1*) or between Δ*lfr1* (*vector*) and Δ*lfr1* (*LFR1*) (Student's *t* test, $p < 0.02$). *D,* wild type and Δ*lfr1* parasites were imaged by differential interference contrast microscopy, and the cell body axis was measured as indicated in the *insets* ($n = 300$). *E,* BMM were infected for 1 h with parasites cultured for 48 h in amastigote growth media (multiplicity of infection = 1.5) and fixed after the indicated periods for determining the number of intracellular parasites. The data represent the mean ± S.D. of the results of three independent experiments. The *asterisk* indicates significant differences when wild type (*vector*) was compared with Δ*lfr1* (*vector*), wild type (*LFR1*), or Δ*lfr1* (*LFR1*) (Student's *t* test, $p < 0.01$). *F* and *G,* BALB/c mice were inoculated in the left hind footpad with 1×10^6 wild type or Δ*lfr1* purified metacyclic forms. *F,* lesion development was measured by weekly caliper measurements. The data correspond to the mean ± S.D. of values from five mice. The *asterisks* indicate significant differences between wild type (*vector*) and Δ*lfr1* (*vector*) (Student's *t* test, $p < 0.0002$). *G,* parasite loads were determined by limiting dilution in footpads of mice inoculated with wild type or Δ*lfr1*. The *asterisks* indicate significant differences between wild type (*vector*) and Δ*lfr1* (*vector*) (Student's *t* test, $p < 0.003$).

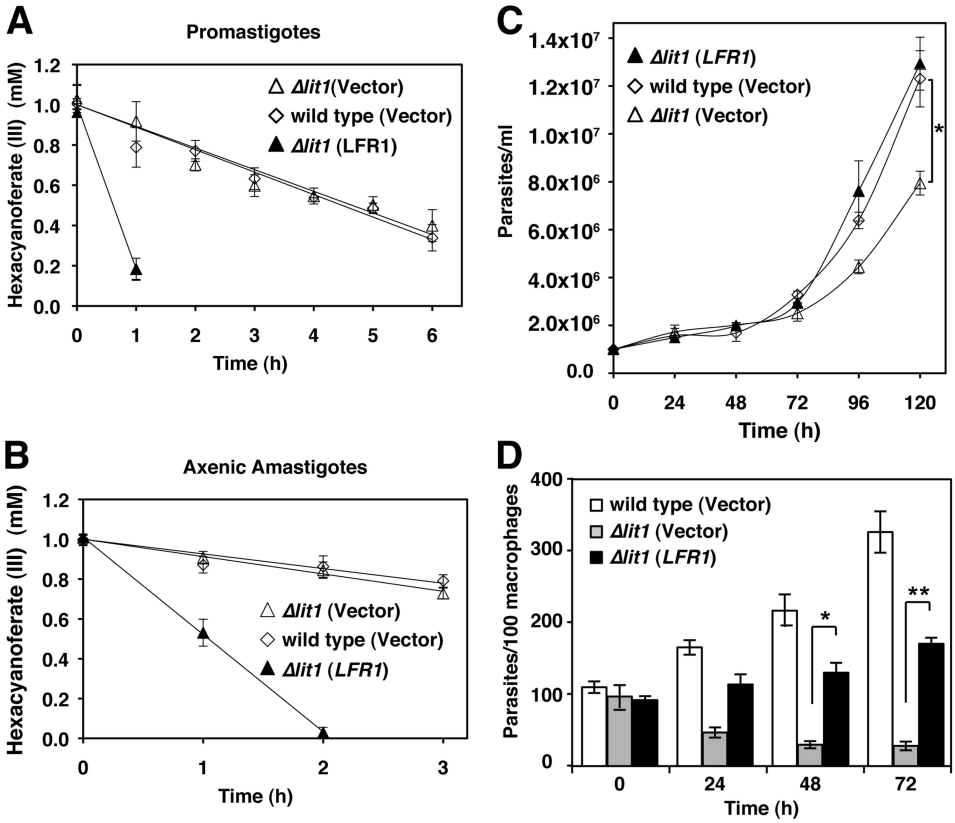

FIGURE 7. **Overexpression of *LFR1* in *LIT1* null *L. amazonensis* is not toxic and rescues axenic and intracellular replication of amastigotes.** Wild type and Δ*lit1 L. amazonensis* promastigotes were transfected with vector alone or pLFR1-SAT. Mid-log phase promastigotes and axenically grown amastigotes were washed and transferred to promastigote or amastigote media lacking hemin, respectively. After 15 h at 26 °C (*A,* promastigotes) or 32 °C (*B,* amastigotes), parasites were washed and assayed for ferric reductase activity at 1×10^8 parasites/ml. The data represent the mean ± S.D. of triplicate determinations and are representative of at least four independent experiments. *B,* axenic amastigotes from wild type (◇) and Δ*lit1* (△) promastigotes transfected with vector alone had similar ferric reductase activity, and Δ*lit1* amastigotes transfected with pLFR1-SAT (▲) had increased ferric reductase activity. *C,* growth rates of wild type (◇) and Δ*lit1* (△) *L. amazonensis* axenic amastigotes transfected with pXG-SAT vector alone and Δ*lit1* transfected with pLFR1-SAT (▲). Overexpression of *LFR1* gene is not deleterious to growth of Δ*lit1* parasites and complements the growth defect seen in Δ*lit1* transfected with vector alone. The data represent the mean ± S.D. of triplicate determinations. The *asterisk* indicates a significant difference between wild type (*vector*) and Δ*lit1* (*vector*) (Student's *t* test, $p < 0.01$). *D,* BMM were infected (multiplicity of infection = 1.0) for 1 h with axenic amastigotes (wild type and Δ*lit1* parasites transfected with vector alone or Δ*lit1* parasites transfected with pLFR1-SAT) and fixed after the indicated incubation periods for determining the number of intracellular parasites. The data represent the mean ± S.D. of the results of three independent experiments. The *asterisks* indicate significant differences between Δ*lit1* (*vector*) and Δ*lit1* (*LFR1*) (Student's *t* test 48 h, $p < 0.01$; 72 h, $p < 0.001$).

DISCUSSION

Evidence has been accumulating in support of the notion that *Leishmania* spp. can obtain iron from a variety of sources, including heme, hemoglobin, transferrin, lactoferrin, or ferric nitrilotriacetate (36–40). However, unlike mammalian cells, these protozoan parasites do not appear to utilize a receptor-mediated mechanism for the uptake of Fe^{3+} chelated to carrier proteins such as transferrin (6, 9, 40). Rather, *Leishmania* directly translocates iron across their plasma membrane through LIT1, a ZIP family Fe^{2+} membrane transporter that is expressed on the plasma membrane of *L. amazonensis* under conditions of iron deprivation (7). LIT1-deficient parasites are unable to replicate within host macrophages and do not cause skin lesions in mice, indicating that this pathway of iron acquisition is essential for the ability of *Leishmania* to cause disease (7).

Ferrous iron transporters are expected to work in concert with ferric reductases, which are essential for the generation of the soluble Fe^{2+} substrate for membrane translocation (4). Indeed, earlier studies using membrane-impermeable substrates detected an NADPH-dependent ferric reductase activity associated with intact promastigote stages of *L. chagasi*, suggesting a plasma membrane association for this enzyme (9). In this study, we have identified *LFR1*, a gene induced under low iron availability that accounts for all the detectable ferric iron reductase activity associated with the surface of *L. amazonensis* promastigotes. The *LFR1* gene and the surface-associated ferric reductase activity are present in several *Leishmania* species, including *L. infantum*, *L. chagasi*, and *L. donovani*, species that cause visceralizing disease (Fig. 1*B*). Interestingly, under the culture conditions utilized, the species causing visceralizing infections expressed lower levels of LFR1 activity than the species that induce cutaneous lesions. This observation suggests the existence of differences in iron acquisition and homeostasis pathways that might be associated with the different environments encountered by the parasites *in vivo*. The characterization of *LFR1* null mutants performed in this study indicates that the ferric reductase LFR1 is essential for the ability of *Leishmania* to differentiate into infective forms and to establish infections.

LFR1 is predicted to have multiple transmembrane domains, a bis-heme-binding motif and a cytoplasmic loop that includes

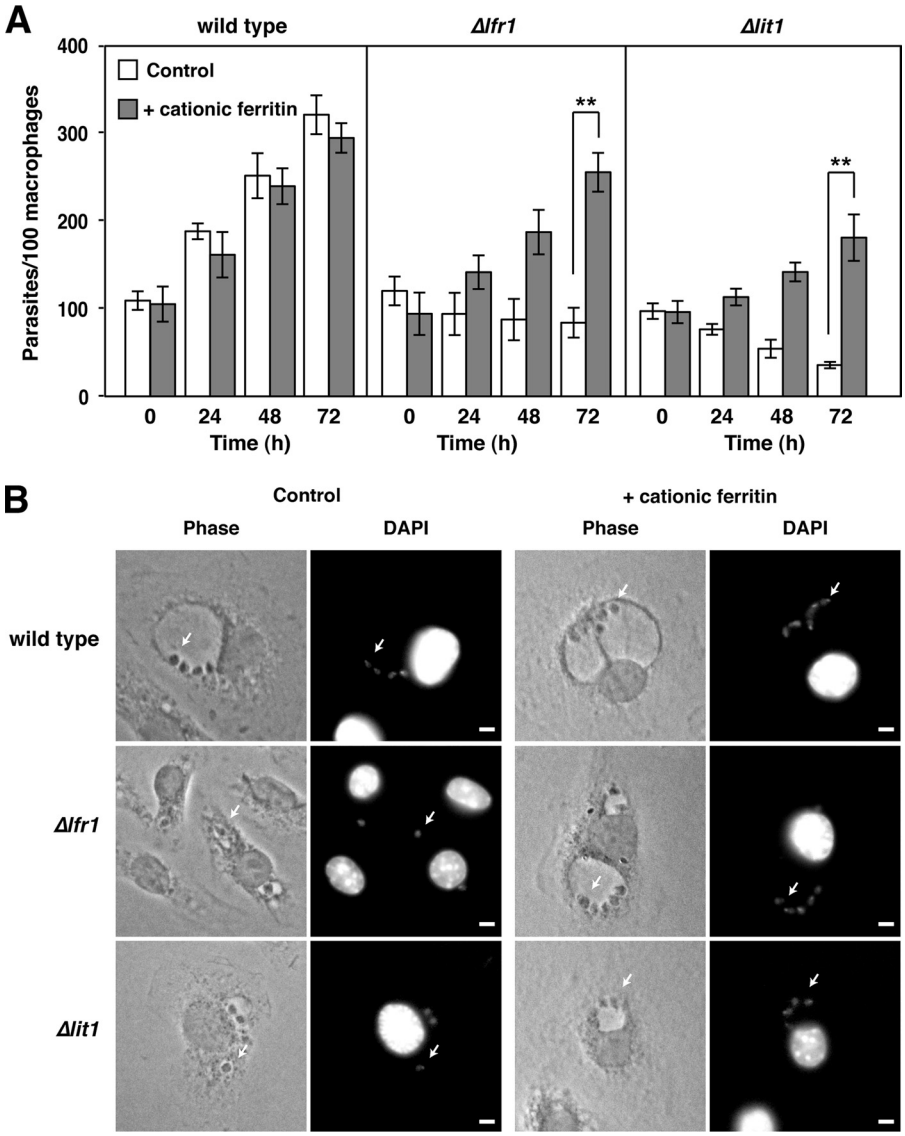

FIGURE 8. **Endocytic pathway loading with cationic ferritin rescues the intracellular growth of *LFR1* null and *LIT1* null *L. amazonensis*.** *A*, BMM were pretreated for 1 h with fresh BMM medium (control) or BMM medium supplemented with 10 μg/ml cationic ferritin. BMM were infected (multiplicity of infection = 1.0) for 1 h with wild type, Δ*lfr1*, or Δ*lit1* axenic amastigotes. The BMM were washed, incubated in fresh BMM medium or BMM medium supplemented with 10 μg/ml cationic ferritin, and fixed after the indicated periods for determining the number of intracellular parasites. The data represent the mean ± S.D. of the results of three independent experiments. The *asterisks* indicate significant differences between the growth of Δ*lfr1* or Δ*lit1* parasites in BMM media *versus* BMM media supplemented with cationic ferritin (Student's *t* test, $p < 0.0\,01$). *B*, phase contrast and DAPI-stained fluorescent images of BMM supplemented with or without cationic ferritin and infected with wild type, Δ*lfr1*, or Δ*lit1* amastigotes at 48 h. The *arrows* indicate intracellular amastigotes. *Scale bars*, 5 μm.

FAD- and NADH-binding sites (Fig. 1*A* and supplemental Fig. S2). These three motifs are a hallmark of the large family of NADPH oxidases, of which one of the best characterized members is GP91-phox, a protein essential for superoxide production by phagocytes (supplemental Fig. S2) (41). NADPH oxidase proteins transfer electrons from NADPH in the cytosol, across the lipid bilayer via the noncovalently bound FAD and histidine-coordinated heme to an acceptor molecule on the outer face of the membrane (42). In the case of the GP91-phox, the acceptor molecule is molecular oxygen, and for ferric reductases the electron acceptor is Fe^{3+}, which is converted to Fe^{2+} (28, 43–45).

The *Leishmania* LFR1 protein shows close similarity to the ferric reductases of *A. thaliana* (FRO1 and FRO2) and *P. sativum* (FRO1) that are involved in root iron acquisition (28, 29, 45). *LIT1*, the only additional *Leishmania* gene identified to date with a role in iron acquisition, was also identified based on its close similarity to an *Arabidopsis* gene, the ZIP family ferrous iron transporter *IRT1*. Interesting questions regarding the phylogenetic origin of genes involved in iron acquisition and homeostasis in these ancient trypanosomatid protozoa are likely to emerge, as soon as additional genes involved in these pathways are identified.

Despite its severe defect in differentiation into infective life cycle stages, *LFR1* null mutants grow normally as promastigotes, the insect forms that can be axenically cultivated in the presence of abundant sources of iron. Because LFR1 expression is up-regulated upon iron deprivation, it is con-

ceivable that in iron-abundant environments *Leishmania* spp. utilizes low affinity iron transport systems, as described for *S. cerevisiae* (4). Alternatively, cultured promastigotes may be able to internalize iron in a form that is independent of Fe^{3+} to Fe^{2+} conversion by a plasma membrane ferric reductase. *Leishmania* parasites are heme auxotrophs, and promastigotes have been proposed to have plasma membrane receptors and/or transporters that mediate heme uptake (36, 38), raising the possibility that heme can serve as a source of iron for these parasites.

Under conditions that promote differentiation into metacyclic promastigotes or axenic amastigotes, the essential role of LFR1 in *L. amazonensis* becomes evident. Without the LFR1 reductase, even in the presence of abundant sources of iron, differentiation into infective stages is incomplete, and viability is reduced. Because overexpression of *LFR1* inhibits parasite growth and reduces viability, we could not directly demonstrate with complementation assays that the differentiation defects of the null mutant are directly attributable to the absence of LFR1. However, taking advantage of the ability to load macrophage endosomal compartments with exogenous iron, we were able to rescue the intracellular growth of *LFR1* null parasites. This result indicates that under excess iron availability, the need for reduction of Fe^{3+} to Fe^{2+} by LFR1 can be bypassed, possibly through the generation of Fe^{2+} by the lysosomal reductase cytochrome b_{561} (46). In addition, utilizing a null mutant lacking the LIT1 Fe^{2+} transporter (7), we showed that LFR1 overexpression rescues the growth defect of *LIT1* null amastigotes, perhaps by providing additional substrate for alternative lower affinity Fe^{2+} transporters. This result provides strong evidence in support of the hypothesis that LFR1 functions upstream of LIT1 by generating the ferrous form of iron that can be transported across the parasite's membrane. Furthermore, our results strongly suggest that the toxicity of LFR1 overexpression is a direct consequence of increased Fe^{2+} production. Without LIT1 to transport Fe^{2+} intracellularly, LFR1 overexpression is no longer toxic, which allowed us to demonstrate that LFR1 can compensate for the growth defect of *LIT1* null mutant amastigotes. Taken together, our results show that the *Leishmania* transmembrane protein LFR1 functions as a ferric iron reductase, converting extracellular chelated Fe^{3+} into the soluble Fe^{2+} form, which is then transported into the parasites by the ZIP family transporter LIT1.

Acknowledgments—We are grateful to Dr. D. L. Sacks (NIAID, National Institutes of Health) for providing the different Leishmania isolates and for helpful discussions and to Dr. J. Kaplan (University of Utah) for useful suggestions. We also thank Drs. L. A. Rodrigues and B. Kachar (NIDCD, National Institutes of Health) for providing technical help and access to the FE-scanning electron microscope and Dr. D. McMahon-Pratt (Yale University) for the anti-P4 antibodies.

REFERENCES

1. Sacks, D., and Kamhawi, S. (2001) *Annu. Rev. Microbiol.* **55,** 453–483
2. Morris, C. J., Earl, J. R., Trenam, C. W., and Blake, D. R. (1995) *Int. J. Biochem. Cell Biol.* **27,** 109–122
3. Imlay, J. A., Chin, S. M., and Linn, S. (1988) *Science* **240,** 640–642
4. Askwith, C. C., de Silva, D., and Kaplan, J. (1996) *Mol. Microbiol.* **20,** 27–34
5. Wu, H., Li, L., Du, J., Yuan, Y., Cheng, X., and Ling, H. Q. (2005) *Plant Cell Physiol.* **46,** 1505–1514
6. Huynh, C., and Andrews, N. W. (2008) *Cell. Microbiol.* **10,** 293–300
7. Huynh, C., Sacks, D. L., and Andrews, N. W. (2006) *J. Exp. Med.* **203,** 2363–2375
8. Jacques, I., Andrews, N. W., and Huynh, C. (2010) *Mol. Biochem. Parasitol.* **170,** 28–36
9. Wilson, M. E., Lewis, T. S., Miller, M. A., McCormick, M. L., and Britigan, B. E. (2002) *Exp. Parasitol.* **100,** 196–207
10. Courret, N., Prina, E., Mougneau, E., Saraiva, E. M., Sacks, D. L., Glaichenhaus, N., and Antoine, J. C. (1999) *Eur. J. Immunol.* **29,** 762–773
11. Pinto-da-Silva, L. H., Fampa, P., Soares, D. C., Oliveira, S. M., Souto-Padron, T., and Saraiva, E. M. (2005) *Int. J. Parasitol.* **35,** 757–764
12. Medina-Acosta, E., and Cross, G. A. (1993) *Mol. Biochem. Parasitol.* **59,** 327–329
13. Marchler-Bauer, A., Anderson, J. B., Chitsaz, F., Derbyshire, M. K., DeWeese-Scott, C., Fong, J. H., Geer, L. Y., Geer, R. C., Gonzales, N. R., Gwadz, M., He, S., Hurwitz, D. I., Jackson, J. D., Ke, Z., Lanczycki, C. J., Liebert, C. A., Liu, C., Lu, F., Lu, S., Marchler, G. H., Mullokandov, M., Song, J. S., Tasneem, A., Thanki, N., Yamashita, R. A., Zhang, D., Zhang, N., and Bryant, S. H. (2009) *Nucleic Acids Res.* **37,** D205–D210
14. Marchler-Bauer, A., and Bryant, S. H. (2004) *Nucleic Acids Res.* **32,** W327–W331
15. Hirokawa, T., Boon-Chieng, S., and Mitaku, S. (1998) *Bioinformatics* **14,** 378–379
16. Chenna, R., Sugawara, H., Koike, T., Lopez, R., Gibson, T. J., Higgins, D. G., and Thompson, J. D. (2003) *Nucleic Acids Res.* **31,** 3497–3500
17. Ha, D. S., Schwarz, J. K., Turco, S. J., and Beverley, S. M. (1996) *Mol. Biochem. Parasitol.* **77,** 57–64
18. LeBowitz, J. H., Coburn, C. M., McMahon-Pratt, D., and Beverley, S. M. (1990) *Proc. Natl. Acad. Sci. U.S.A.* **87,** 9736–9740
19. Depledge, D. P., Evans, K. J., Ivens, A. C., Aziz, N., Maroof, A., Kaye, P. M., and Smith, D. F. (2009) *PLoS Negl. Trop. Dis.* **3,** e476
20. Rochette, A., Raymond, F., Ubeda, J. M., Smith, M., Messier, N., Boisvert, S., Rigault, P., Corbeil, J., Ouellette, M., and Papadopoulou, B. (2008) *BMC Genomics* **9,** 255
21. Olakanmi, O., Stokes, J. B., Pathan, S., and Britigan, B. E. (1997) *J. Biol. Chem.* **272,** 2599–2606
22. Goldberg, M. W., and Allen, T. D. (1992) *J. Cell Biol.* **119,** 1429–1440
23. Kar, S., Soong, L., Colmenares, M., Goldsmith-Pestana, K., and McMahon-Pratt, D. (2000) *J. Biol. Chem.* **275,** 37789–37797
24. Becker, S. M., Delamarre, L., Mellman, I., and Andrews, N. W. (2009) *Immunobiology* **214,** 495–505
25. Tabbara, K. S., Peters, N. C., Afrin, F., Mendez, S., Bertholet, S., Belkaid, Y., and Sacks, D. L. (2005) *Infect. Immun.* **73,** 4714–4722
26. Finn, R. D., Mistry, J., Tate, J., Coggill, P., Heger, A., Pollington, J. E., Gavin, O. L., Gunasekaran, P., Ceric, G., Forslund, K., Holm, L., Sonnhammer, E. L., Eddy, S. R., and Bateman, A. (2010) *Nucleic Acids Res.* **38,** D211–D222
27. Dancis, A., Roman, D. G., Anderson, G. J., Hinnebusch, A. G., and Klausner, R. D. (1992) *Proc. Natl. Acad. Sci. U.S.A.* **89,** 3869–3873
28. Waters, B. M., Blevins, D. G., and Eide, D. J. (2002) *Plant Physiol.* **129,** 85–94
29. Schagerlöf, U., Wilson, G., Hebert, H., Al-Karadaghi, S., and Hägerhäll, C. (2006) *Plant Mol. Biol.* **62,** 215–221
30. Finegold, A. A., Shatwell, K. P., Segal, A. W., Klausner, R. D., and Dancis, A. (1996) *J. Biol. Chem.* **271,** 31021–31024
31. Sacks, D. L., and Perkins, P. V. (1984) *Science* **223,** 1417–1419
32. Hodgkinson, V. H., Soong, L., Duboise, S. M., and McMahon-Pratt, D. (1996) *Exp. Parasitol.* **83,** 94–105
33. Titus, R. G., Marchand, M., Boon, T., and Louis, J. A. (1985) *Parasite Immunol.* **7,** 545–555
34. Anderson, E., and Batten, B. E. (1983) *Tissue Cell* **15,** 853–871
35. Radisky, D. C., and Kaplan, J. (1998) *Biochem. J.* **336,** 201–205
36. Chang, C. S., and Chang, K. P. (1985) *Mol. Biochem. Parasitol.* **16,** 267–276
37. Segovia, M., Navarro, A., and Artero, J. M. (1989) *Ann. Trop. Med. Parasitol.* **83,** 357–360

38. Sengupta, S., Tripathi, J., Tandon, R., Raje, M., Roy, R. P., Basu, S. K., and Mukhopadhyay, A. (1999) *J. Biol. Chem.* **274,** 2758–2765
39. Soteriadou, K., Papavassiliou, P., Voyiatzaki, C., and Boelaert, J. (1995) *J. Antimicrob. Chemother.* **35,** 23–29
40. Wilson, M. E., Vorhies, R. W., Andersen, K. A., and Britigan, B. E. (1994) *Infect. Immun.* **62,** 3262–3269
41. Sumimoto, H. (2008) *FEBS J.* **275,** 3249–3277
42. Cross, A. R., and Segal, A. W. (2004) *Biochim. Biophys. Acta* **1657,** 1–22
43. Anderson, G. J., Lesuisse, E., Dancis, A., Roman, D. G., Labbe, P., and Klausner, R. D. (1992) *J. Inorg. Biochem.* **47,** 249–255
44. Shatwell, K. P., Dancis, A., Cross, A. R., Klausner, R. D., and Segal, A. W. (1996) *J. Biol. Chem.* **271,** 14240–14244
45. Vasconcelos, M., Eckert, H., Arahana, V., Graef, G., Grusak, M. A., and Clemente, T. (2006) *Planta* **224,** 1116–1128
46. Zhang, D. L., Su, D., Bérczi, A., Vargas, A., and Asard, H. (2006) *Biochim. Biophys. Acta* **1760,** 1903–1913